JMEPEG (2009) 18:569–574
DOI: 10.1007/s11665-009-9351-8

1059-9495/$19.00

Fracture Behaviour of Nickel-Titanium Laser Welded Joints

C. Maletta, A. Falvo, F. Furgiuele, G. Barbieri, and M. Brandizzi

(Submitted October 6, 2008; in revised form December 2, 2008)

In this study, the effects of Nd:YAG laser welding on the fracture behavior of Ni-rich nickel-titanium sheets are analyzed by experimental investigations. The welding was carried out in open air conditions by using a special shielding/clamping system to avoid the chemical contamination of the molten zone and the formation of hot cracks. Mechanical tests of standard dog bone-shaped and single edge crack specimens were carried out to measure the stress-strain response and the fracture resistance of both the base and the welded materials. Furthermore, scanning electron microscopy observations of the fracture surfaces were carried out in order to better understand the failure mechanisms. Finally, systematic comparative studies between base and laser-welded materials were carried out.

Keywords Fracture mechanics, Mechanical Testing, Shape Memory Alloys (SMAs), Welding

1. Introduction

Nickel-Titanium-based (NiTi) Shape Memory Alloys (SMAs) have seen growing applications in recent years in many branches of engineering, due to their special functional properties; namely Shape Memory Effect (SME) and Superelastic Effect (SE) (Ref 1). These properties are due to a solid-state phase transformation between martensite and austenite, the so-called Thermoelastic Martensitic Transformation (TMT), which can be activated by thermal or mechanical loads. Furthermore, the demand for NiTi alloys is expected to rise considerably in the near future due to the reductions in manufacturing costs and improvements in product quality. However, due to the low formability of these alloys, suitable joining and cutting techniques must be used to obtain devices and components with complex geometries. In fact, the functional properties of NiTi alloys are strongly affected by the modifications induced by the working processes, in terms of thermo-mechanical effects and chemical contaminations (Ref 1), and a deeper understanding of these modifications could be useful for developing new industrial applications. In this field, obtaining welded joints with similar mechanical and functional properties of the base material, could create new possibilities for the realization of complex-shaped components.

This article is an invited paper selected from presentations at Shape Memory and Superelastic Technologies 2008, held September 21-25, 2008, in Stressa, Italy, and has been expanded from the original presentation.

C. Maletta, A. Falvo, and **F. Furgiuele**, Department of Mechanical Engineering, University of Calabria, Arcavacata Rende, CS, Italy; **G. Barbieri**, CR ENEA Casaccia, Rome, Italy; and **M. Brandizzi**, Consorzio CALEF, CR ENEA Trisaia, Matera, Italy. Contact e-mail: carmine.maletta@unical.it.

Laser welding is one of the most important joining techniques for this class of materials, and in particular the Nd:YAG source is suitable for welding low-thickness components due to an accurate control of the welding power, resulting in a reduced heat-affected zone (HAZ) (Ref 2-4). However, two major drawbacks arise during welding of NiTi alloys: (i) the chemical contamination of the joint, mainly due to the high oxidation rate of titanium, and (ii) the formation of hot cracks in the molten zone, due to the thermal shrinkage of the material during the cooling stage after welding. Therefore, an efficient protection of the molten zone, by inert gas, and an accurate positioning of the components to be welded, are of major concern in order to obtain welded joints with satisfactory mechanical and functional properties. For these reasons, some research activities have been carried out in the last few years to evaluate the effects of laser welding on the mechanical and functional properties of NiTi alloys (Ref 2-7).

Unfortunately, few experimental research programs have been devoted to the fracture mechanics of NiTi alloys (Ref 8-11), i.e., to study the mechanical behavior of cracked components. This topic is particularly interesting because the stress singularity around the crack tip activates the Stress-Induced Martensitic (SIM) transformation (Ref 8-13), which significantly changes the stress distribution in the crack tip region with respect to common engineering metals and, consequently, plays a critical role in the fracture toughness of the material. Furthermore, no research, to the knowledge of the authors, has been carried out to study the fracture mechanics of NiTi welded joints.

In this article, the effects of Nd:YAG laser welding on the fracture behavior of Ni-49.2 at.% Ti sheets were analyzed by experimental investigations. The welding was carried out in open air conditions, i.e., without using closed shielding chambers, by special dynamic shielding equipment and a positioning/clamping system to overcome the aforementioned drawbacks.

The stress-strain responses of both the welded and the base (reference) materials, were measured by using dog bone-shaped specimens, while the fracture resistance was analyzed by Single Edge Crack (SEC) specimens. The test specimens were cut

from reference and previously welded sheets, using a water jet technique, and the pre-cracks in the SEC specimens were made by electro-discharge machining (EDM). Furthermore, Scanning Electron Microscopy (SEM) observations of the fracture surface were carried out in order to better understand the failure mechanisms of both the reference and the welded specimens. Finally, systematic comparisons of the results between the base and the laser-welded materials were carried out.

2. Materials and Experiments

Ni-49.2 at.% Ti sheets with oxide-free surfaces and a thickness of 0.75 mm (Type S, Memory Metalle, Germany) were used in this investigation. The material has a nominal austenite finish temperature $A_f = -7$ °C, and therefore, it exhibits a full austenitic structure at room temperature.

2.1 Laser-Welding Process

The welding process was carried out by a Nd:YAG laser source (Trumpf HL2006D) with a maximum power of 2 kW. Special systems for open-air laser welding, illustrated in Fig. 1, were used in order to overcome the main drawbacks which arise during welding NiTi alloys, such as the chemical contamination of the joint and the formation of hot cracks. In particular, a dynamic shielding system allows an efficient protection of the top side of the molten zone by an inert buffer state, which is generated by blowing argon gas through a perforated plate during welding. Furthermore, a special system was used, which allows an accurate positioning of the components to be welded and applies a compressive force to the joint in order to avoid the formation of hot cracks; in addition, an inert gas delivery system protects the back side of the molten zone from the oxidation.

The welding was executed in continuous mode and a set of preliminary tests were carried out in order to identify the optimal values of the process parameters, as illustrated in the following sections.

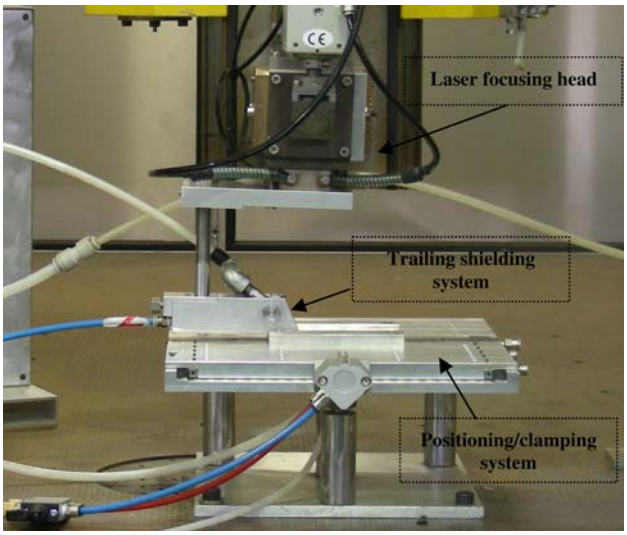

Fig. 1 Open-air laser welding equipments: (a) dynamic top shielding system; (b) positioning/clamping system

2.2 Specimen Preparation and Mechanical Testing

Two types of specimens were used for mechanical tests, a dog bone-shaped for stress-strain measurements (see Fig. 2a) and a SEC for fracture tests (see Fig. 2b).

Due to the poor workability of NiTi alloys with conventional cutting techniques, the specimens for mechanical tests were made by a water jet cutting technique, which provides a high accuracy with no HAZ.

In Fig. 3, the two types of test specimens are shown, together with a comparison between reference and laser-welded ones. The welded specimens were cut from previously butt-welded sheets, with the weld bead perpendicular to the loading direction and in the middle section of both types of specimens. In particular, Fig. 3(a) illustrates the dog bone-shaped specimens, while Fig. 3(b) illustrates the SEC ones with an highlight of the pre-crack; this latter was made by EDM by using a copper wire with diameter $\phi = 150$ μm, which produces a notch radius of about 80 μm. As clearly illustrated in Fig. 3(b), the pre-cracks were made in the middle of the molten zone of the welded specimens.

The mechanical tests were carried out by using a universal testing machine (Instron 8500), equipped with a furnace (MTS 653) and a resistance extensometer with a gauge length of 10 mm. Both specimens were tested in isothermal conditions, by applying a displacement-controlled monotonic load, at a cross head rate of 0.2 mm/min. Furthermore, a special loading/clamping system was used to avoid spurious loading conditions and premature failure of the specimen in the pin-hole regions.

3. Results

3.1 Microscopic Observations and Vickers Hardness

A set of preliminary tests were carried out in order to identify the optimal values of the process parameters, such as

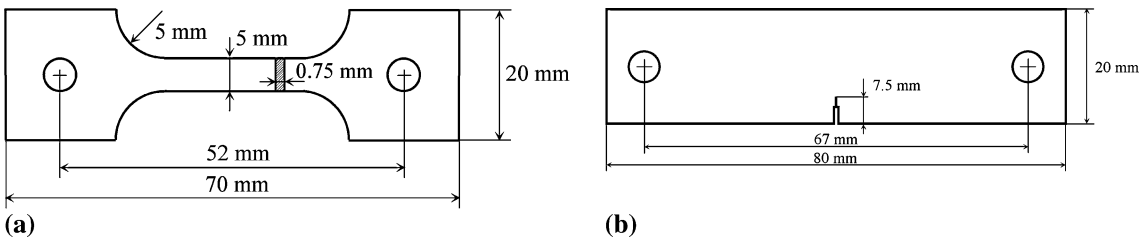

Fig. 2 Specimens for mechanical tests: (a) dog bone-shaped specimen for stress-strain tests; (b) single edge crack specimen for fracture tests

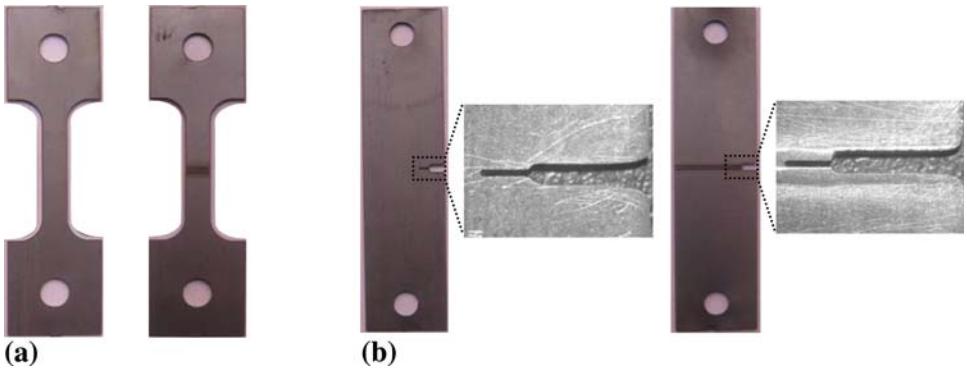

Fig. 3 Reference and welded specimens for mechanical tests: (a) dog bone-shaped specimen; (b) single edge crack with an highlight of the pre-crack

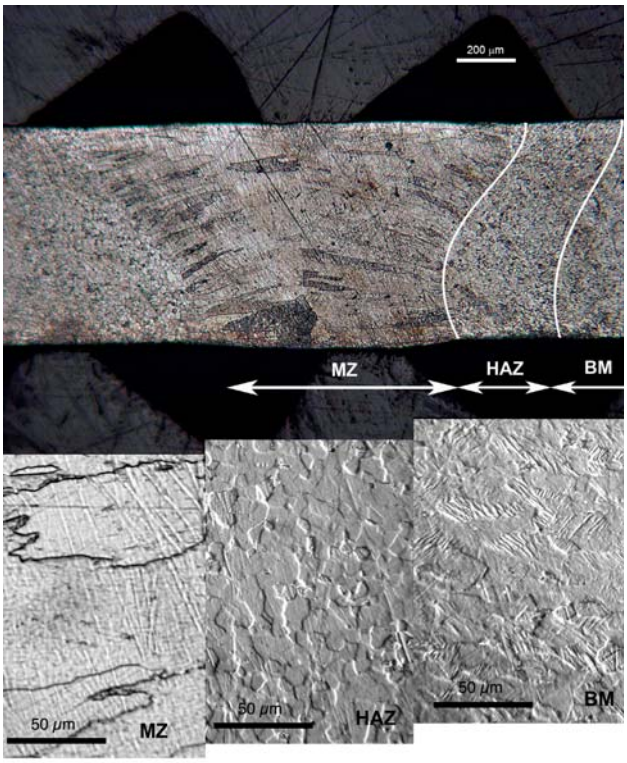

Molten zone	0.8~1.5 mm
Heat affected zone	~0.4 mm

Fig. 4 Light micrographs of the cross section of the weld bead

average power and welding rate. To this aim, microscopic observations and hardness tests were executed to evaluate the extension of the HAZ and molten zone (MZ), obtained by several values of the aforementioned welding parameters. Finally, the following values were chosen: average power of 850 W and welding rate of 2400 mm/min.

Figure 4 illustrates a light micrograph of the cross section of the weld bead together with micrographic observations of the MZ, HAZ, and base material (BM), carried out at higher magnifications. The figure shows a V-shaped MZ with root width of about 0.8 mm and maximum width of about 1.5 mm, and a HAZ of about 0.4 mm.

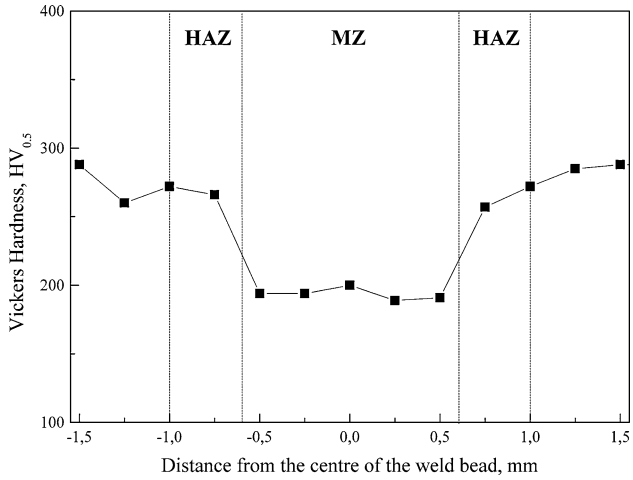

Fig. 5 Hardness profile of a cross section of the weld bead

Figure 5 illustrates the results of the hardness tests, carried out on a cross section of the weld bead by using a Vickers indenter and a weight of 0.5 kg ($HV_{0.5}$), which show an overall reduction of hardness in the molten zone with respect to the base material from about 280 to 190 $HV_{0.5}$.

3.2 Stress-Strain Measurements

Figure 6 illustrates a comparison between the stress-strain curves of the reference and laser welded specimens, obtained from isothermal uniaxial loading tests of dog bone shaped specimens, carried out at room temperature. Three different specimens for each type were analyzed and a high repeatability of the results was found as illustrated in Table 1; this latter reports the average values of the maximum stresses as well as the transformation stresses and strains, together with the standard deviations. Figure 6 and Table 1 clearly illustrate a strong reduction of the maximum stress in the welded specimen with respect to the reference, from about 1250 to 780 MPa, mainly due the modifications induced by the welding. Notwithstanding the reduction in the mechanical strength, the stress-strain transformation behavior of the material seems to be mainly unaffected by the welding, as a similar stress plateau is observed in both materials, i.e., similar values of the transformation stress and strain were measured. In fact, student-*t* test, at a 99% confidence level, indicates no significant differences

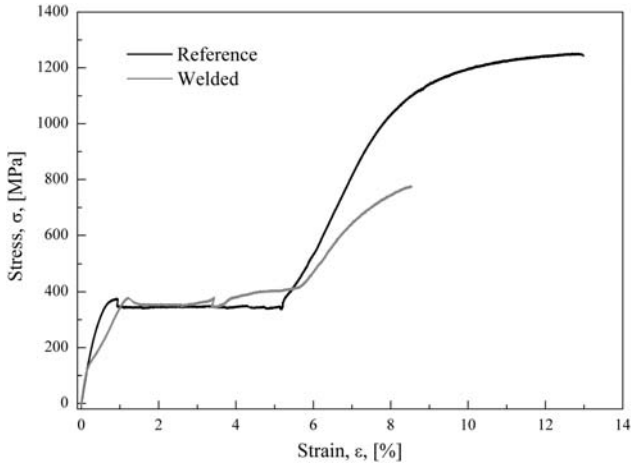

Fig. 6 Comparison between the stress-strain curves of the reference and welded specimens

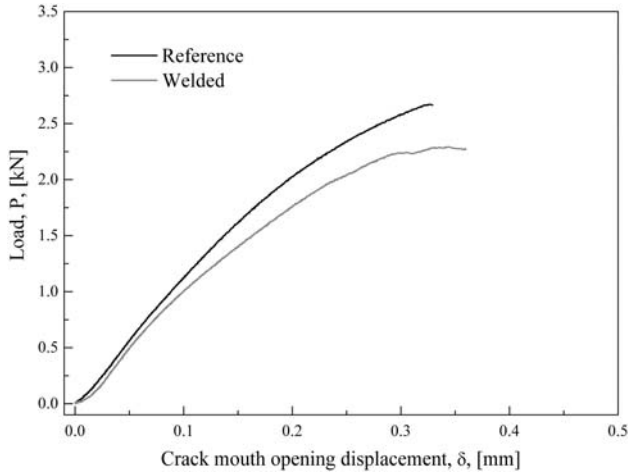

Fig. 7 Comparison between the load versus crack mouth opening displacement curves of the reference and welded specimens

Table 1 Main mechanical and functional parameters of the reference and welded specimens

	Transformation stress, MPa	Transformation strain, %	Maximum stress, MPa
Reference	345 ± 3	4.6 ± 0.1	1248 ± 7
Welded	355 ± 5	4.6 ± 0.3	776 ± 35

between transformation stress and strain in welded and reference specimens. However, it is worth noting that the curves in Fig. 6 illustrate the effective behavior of the joint over a gauge length of 10 mm, while the stress-strain response of the material in the MZ and in the HAZ is expected to be different from the measured one. This observation seems to be confirmed by more detailed comparisons between the stress-strain curves of the reference and laser-welded specimens, which show the following differences: (i) laser welded specimens exhibit a change of the slope in the austenitic region at a stress level lower than the nominal transformation stress and (ii) stress variations are observed in the stress-strain transformation curves of the welded specimens. Notwithstanding that full-field displacement measurements should be carried out in order to better understand the functional behavior of the material in the welded region, the observed differences should be attributed to a different transformation behavior of the material in the MZ and HAZ. In particular, the change of the slope in the early stage of loading and the stress variations in the transformation plateau should be attributed to non-homogeneous transformations, i.e., the stress-induced martensitic transformation in the welded region occurs in a different stress range with respect to the reference material.

3.3 Fracture Tests

Figure 7 illustrates a comparison between the load versus crack mouth opening displacement curves of the reference and laser-welded materials, obtained from isothermal tests of SEC specimens, carried out at room temperature. Three different specimens for each type were tested, and the results are illustrated in Table 2 in terms of maximum load and notch strength. The latter data were computed as the maximum

Table 2 Mechanical strength of the SEC specimens

	Maximum load, kN	Notch strength, MPa
Reference	2.65 ± 0.03	284 ± 3
Welded	2.26 ± 0.05	243 ± 5

nominal stress at failure according to the standard ASTM E338-91 (Ref 14). The table clearly illustrates that the welded specimens exhibit a reduction in the notch strength of about 15% with respect to the reference specimens. Furthermore, student-*t* test, at a 99% confidence level, indicates a significantly different strength between welded and reference specimens.

The fracture path is almost straight along the symmetry plane of both specimens and it is always located in the HAZ of the welded specimens, although the non-symmetric shape of the weld bead causes non-pure mode I loading conditions.

Furthermore, the notch strength is calculated for a comparative analysis between the fracture resistance of the reference and the laser-welded materials, and no further considerations are made about the fracture resistance; in fact, the well-known equations to calculate the stress intensity factor cannot be applied to such class of materials, due to the stress-induced martensitic transformation occurring in the crack tip region, as a consequence of the high values of local stresses, which generate a more complex stress distribution with respect to common engineering metals.

3.4 SEM Observations

In order to better understand the fracture mechanisms of both reference and laser welded materials, the fracture surfaces of the SEC specimens were analyzed by SEM investigations. Figure 8 illustrates the fracture surface of the reference (Fig. 8a, c) and welded specimens (Fig. 8b, d). Figure 8(a) and (b) show the fracture surfaces, together with the pre-cracks (left side) which were made by EDM; the figure indicates a mostly ductile fracture surface in the reference material, while a more brittle fracture mechanism is observed in the welded specimen. This observation is qualitatively confirmed by SEM observation at higher magnification, as illustrated in the

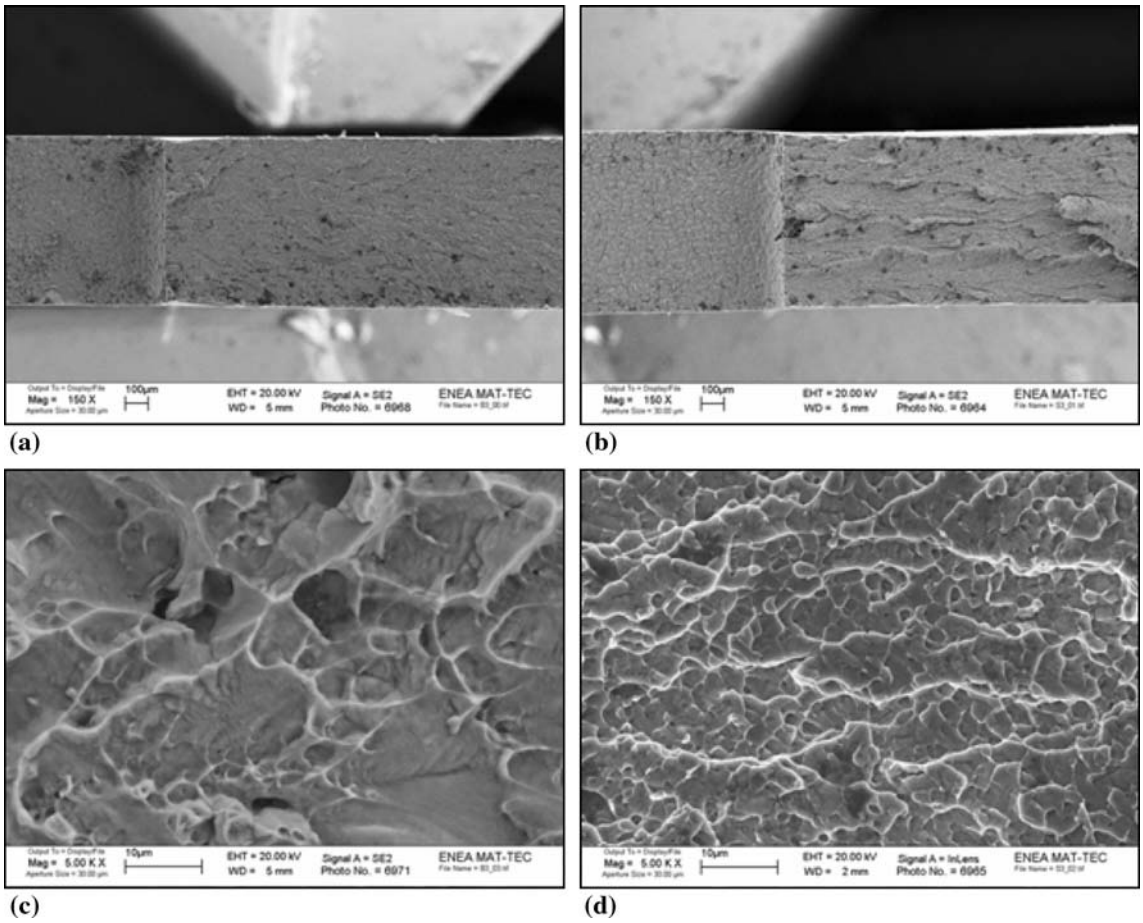

Fig. 8 SEM observation of the fracture surface: (a) reference and (b) welded (magnification: 150×); (c) reference and (d) welded (magnification: 5000×)

Fig. 8(c) and (d), which show dimple size of about 10-30 μm in the reference specimens and about 5 μm in laser-welded ones. Notwithstanding that the dimple sizes could be also affected by different grain size in the welded material, these results indicate a greater plasticization capability in the reference specimens than in the welded ones.

4. Conclusions

Ni-rich nickel-titanium sheets were welded in open-air conditions by a Nd:YAG laser source, and special shielding/positioning systems were used to avoid the chemical contamination of the joints and the formation of hot cracks. The effects of laser welding on the fracture behavior were analyzed by mechanical tests and systematic comparative studies between the base and the welded materials.

The mechanical tests of dog bone-shaped specimens indicate a reduction in the mechanical strength, while the overall functional behavior of the specimens seems to be mainly unaffected by the welding, as a similar stress-strain transformation plateau is observed in both materials.

The tests of single edge crack specimens show a reduction of about 15% in the notch strength of the welded specimens with respect to the reference ones. The fracture path is almost straight along the symmetry plane of both specimens, as a consequence of a pure mode I loading condition, and it is always located in the HAZ of the welded specimens. Furthermore, SEM observations show mostly ductile fracture surfaces in the base material, while a more brittle behavior is observed in the welded one.

Future studies should be carried out in order to better understand the functional behavior of the material in the welded region, by using full-field displacement measurements. Furthermore, for a complete fracture characterization of the material, the stress-induced martensitic transformation which occurs in the crack tip region should be better investigated, by numerical simulations and experimental measurements.

Acknowledgments

This research was supported by the CALEF consortium (Rotondella, Italy), within the framework of the LACER project. Furthermore, the authors wish to thank L. Pilloni (ENEA, Casaccia) and M. B. Alba (ENEA, Trisaia) for their valuable supports in microscopic observations.

References

1. K. Otsuka and X. Ren, Physical Metallurgy of Ti-Ni-based Shape Memory Alloys, *Prog. Mater. Sci.*, 2005, **50**(5), p 511–678

2. A. Tuissi, S. Besseghini, T. Ranucci, F. Squatrito, and M. Pozzi, Effect of Nd-YAG Laser Welding on the Functional Properties of the Ni-49.6at.%Ti, *Mater. Sci. Eng. A*, 1999, **273–275**, p 813–817
3. A. Falvo, F. Furgiuele, and C. Maletta, Laser Welding of a NiTi Alloy: Mechanical and Shape Memory Behaviour, *Mater. Sci. Eng. A*, 2005, **412**(1–2), p 235–240
4. A. Falvo, F. Furgiuele, and C. Maletta, Functional Behaviour of a NiTi Welded Joint: Two Way Shape Memory Effect, *Mater. Sci. Eng. A*, 2008, **481–482**(1–2), p 647–650
5. P. Schlossmacher, T. Haas, and A. Shussler, Laser-Welding of a Ni-Rich TiNi Shape Memory Alloy: Mechanical Behavior, *J. Phys. IV Coll*, 1997, **C 5**, p 251–256
6. P. Schlossmacher, T. Haas, and A. Shussler, Laser Welding of Ni-Ti Shape Memory Alloys, *SMST-94: Proceedings of the 1st International Conference on Shape Memory and Superelastic Technologies*, March 7–10, 1994 (Pacific Grove, CA), p 85–90
7. T. Haas and A. Schuessler, Welding and Joining of TiNi Shape Memory Alloys: Engineering Aspects and Medical Applications, *SMST-99: Proceedings of the 1st European Conference on Shape Memory and Superelastic Technologies*, Sept. 5–6, 1999 (Paris), p 103–114
8. J.H. Chen, W. Sun, and G.Z. Wang, Investigation on the Fracture Behavior of Shape Memory Alloy NiTi, *Metall. Mater. Trans. A*, 2005, **36**, p 941–955
9. S. Gollerthan, D. Herberg, A. Baruj, and G. Eggeler, Compact Tension Testing of Martensitic/Pseudoplastic NiTi Shape Memory Alloys, *Mater. Sci. Eng. A*, 2008, **481–482**, p 156–159
10. S.W. Robertson, A. Mehta, A.R. Pelton, and R.O. Ritchie, Evolution of Crack-tip Transformation Zones in Superelastic Nitinol Subjected to In Situ Fatigue: A Fracture Mechanics and Synchrotron X-ray Microdiffraction Analysis, *Acta Mater.*, 2007, **55**, p 6198–6207
11. M.R. Daymond, M.L. Young, J.D. Almer, and D.C. Dunand, Strain and Texture Evolution During Mechanical Loading of a Crack Tip in Martensitic Shape-memory NiTi, *Acta Mater.*, 2007, **55**, p 3929–3942
12. X.M. Wang, Y.F. Wang, A. Baruj, G. Eggeler, and Z.F. Yue, On the Formation of Martensite in Front of Cracks in Pseudoelastic Shape Memory Alloys, *Mater. Sci. Eng. A*, 2005, **394**, p 393–398
13. G.Z. Wang, A Finite Element Analysis of Evolution of Stress-Strain and Martensite Transformation in Front of a Notch in Shape Memory Alloy NiTi, *Mater. Sci. Eng. A*, 2007, **460–461**, p 383–391
14. "Standard Test Method of Sharp-Notch Tension Testing of High-Strength Sheet Materials," E338-91, *Annual Book of ASTM Standards 03.01*, 1996, p 360–365